Chin. Phys. Lett. **39**, 063701 (2022)

Generalized Aubry–André–Harper Models in Optical Superlattices

Yi Li(李一)[1,2], Jia-Hui Zhang(张佳辉)[1,2], Feng Mei(梅锋)[1,2*], Jie Ma(马杰)[1,2], Liantuan Xiao(肖连团)[1,2], and Suotang Jia(贾锁堂)[1,2]

[1]*State Key Laboratory of Quantum Optics and Quantum Optics Devices, Institute of Laser Spectroscopy, Shanxi University, Taiyuan 030006, China*
[2]*Collaborative Innovation Center of Extreme Optics, Shanxi University, Taiyuan 030006, China*

(Received 29 March 2022; accepted 20 April 2022; published online 29 May 2022)

Ultracold atoms trapped in optical superlattices provide a simple platform for realizing the seminal Aubry–André–Harper (AAH) model. However, this model ignores the periodic modulations on the nearest-neighbor hoppings. We establish a generalized AAH model by which an optical superlattice system can be approximately described when $V_1 \gg V_2$, with periodic modulations on both on-site energies and nearest-neighbor hoppings. This model supports much richer topological properties absent in the standard AAH model. Specifically, by calculating the Chern numbers and topological edge states, we show that the generalized AAH model possesses multifarious topological phases and topological phase transitions, unlike the standard AAH model supporting only a single topological phase. Our findings can uncover more opportunities for using optical superlattices to study topological and localization physics.

DOI: 10.1088/0256-307X/39/6/063701

Ultracold atoms in optical lattices have been established as a powerful platform for exploring the topological phases of matter in the last decades.[1–3] This platform features unprecedented controllability and flexibility, opening the possibilities for going beyond the standard solid-state topological systems. For example, ultracold atoms allow the creation of a synthetic inner dimension.[4,5] The basic idea is that by coupling sets of atomic states sequentially, ranging from internal hyperfine,[6,7] magnetic,[8] clock[9–11] and Rydberg states,[12] to external momentum,[13,14] orbital[15] and superradiant states,[16–20] one can construct a synthetic dimension which treats the atomic states as lattice sites and the couplings between them as the lattice hoppings. This approach enables the implementation of high-dimensional topological models in low-dimensional optical lattices with a synthetic real-space dimension. Moreover, it provides opportunities for exploring the previously challenging topological effects, such as the realization of chiral edge states in optical lattices[6,7] and Laughlin's topological pump.[21]

The concept of synthetic dimension can also be generalized to the momentum space. By exploiting high controllability in optical lattices, one can regard a periodic systematic parameter as extra momentum, building a synthetic momentum space by tuning such a parameter from 0 to 2π. Recent studies have shown that optical superlattices offer a natural platform for realizing such a synthetic dimension.[22,23] This superlattice is created by superimposing a long optical lattice on a short one, both produced by standing-wave lasers. The corresponding tight-binding Hamiltonian is naturally described using the seminal Aubry–André–Harper (AAH) model.[24,25] Since the two standing-wave lasers have incommensurate wavelengths, the incommensurate AAH model[24,25] well known for displaying the Anderson localization transition[25–39] can be implemented, enabling the observation of the Anderson localization of the Bose–Einstein condensate.[40] In the commensurate case, this one-dimensional model supports multiple energy bands. It can be mapped into two dimensions by associating the relative phase of the two standing-wave lasers as synthetic momentum, allowing us to study the topological properties of the two-dimensional integer quantum Hall insulator[22,41] and Z_2 topological insulator phases.[23]

We observed that previous works have focused on an extreme case where the periodic modulations on the nearest-neighbor hoppings were ignored, which leads to the desired standard AAH model with only on-site periodic modulations.[22,23,40] In this Letter, we highlight that the corresponding optical superlattice system realizes a generalized AAH model in the limiting case $V_1 \gg V_2$, with periodic modulations on both the on-site energies and nearest-neighbor hoppings. We present the detailed derivation for this model, from the single-particle Hamiltonian to the approximated tight-binding Hamiltonian. The one-dimensional generalized AAH model can be mapped to a two-dimensional lattice model describing a gen-

*Corresponding author. Email: meifeng@sxu.edu.cn
© 2022 Chinese Physical Society and IOP Publishing Ltd

eralized integer quantum Hall effect by regarding the relative laser phase as a synthetic momentum and considering the commensurate case. Based on calculating the Chern numbers and topological edge states, we demonstrate that this model holds much richer topological properties absent in the standard AAH model, including multiple topological phases and different topological edge states.

Compared to previous studies on off-diagonal AAH models,[42–44] our study shows that the generalized AAH model presented here could support multiple multi-band topological phases and various topological phase transitions, unreported previously. Particularly for when the AAH models support an even number of energy bands, our studies show that the two middle bands correspond to the nontrivial gapped topological phases, whereas in previous studies, these two middle bands are gapless topological phases.[42–44] Moreover, extending the generalized AAH model to the incommensurate case could offer opportunities beyond the standard AAH model for studying its underlying localization features.[45,46]

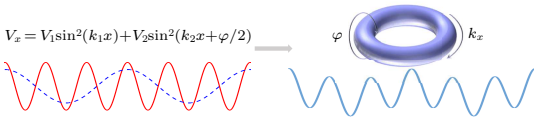

Fig. 1. Schematic illustration of the optical superlattice created by superimposing two standing-wave lasers. By regarding the relative laser phase φ as a synthetic dimension, such a one-dimensional lattice allows the exploration of nontrivial topological properties attributed to systems in two dimensions.

Generalized Aubry–André–Harper models in Optical Superlattices. The optical superlattice with an ultracold atom trapped inside is created by superimposing a short and long optical lattice, as shown in Fig. 1, where two standing-wave lasers respectively produce the two optical lattice potentials. The resulting optical superlattice potential takes the following form:

$$V_x = V_1 \sin^2(k_1 x) + V_2 \sin^2(k_2 x + \varphi/2), \tag{1}$$

where $V_{1,2}$ are the strengths of the short and long optical lattice potentials, respectively; $k_{1,2} = 2\pi/\lambda_{1,2}$ are the corresponding laser wave vectors, and φ is the relative phase of the two lasers. Throughout this study, we assumed that V_1 is larger than V_2. Thus, the short lattice is the primary lattice, determining the period of the whole optical superlattice $a = \lambda_1/2$, and the long lattice is a perturbation, modulating the nearest-neighbor hoppings and on-site energies.

The single-particle Hamiltonian for the short optical lattice system is written as

$$\hat{H}_{s1} = \frac{p_x^2}{2\,m} + V_1 \sin^2(k_1 x). \tag{2}$$

In the second quantization, the continuum single-particle Hamiltonian $H_{\rm s}$ is transformed into

$$\hat{H}_1 = \int dx \psi^+(x) \hat{H}_{s1} \psi(x). \tag{3}$$

Here we assume that atoms are trapped in the ground band. The field operator is expanded as

$$\psi(x) = \sum_m c_m W(x - x_m). \tag{4}$$

Here c_m is the annihilation operator at the lattice site x_m, and $W(x - x_m)$ is the corresponding ground band Wannier function. The lattice spacing is assumed as $a = 1$ throughout this study. By substituting Eq. (4) into Eq. (3), we obtain the tight-binding Hamiltonian

$$\hat{H}_1 = \sum_m t_0 \left(c_m^\dagger c_{m+1} + \text{H.c.}\right), \tag{5}$$

where

$$t_0 = \int dx W^*(x - x_m) \left(\frac{p_x^2}{2\,m} + V_1 \sin^2(k_1 x)\right) \cdot W(x - x_{m+1}). \tag{6}$$

The single-particle Hamiltonian for the long lattice is

$$\hat{H}_{s2} = V_2 \sin^2(k_2 x + \varphi/2). \tag{7}$$

Since $V_1 \gg V_2$, the long lattice does not substantially change the minimal position of the short lattice. Thus, the field operator can still be approximately expanded in the basis of the Wannier states defined in terms of the short lattice. With this approximation, we can easily obtain the expression of the tight-binding Hamiltonian for the whole optical superlattice system. Using the same procedure for obtaining H_1, the tight-binding Hamiltonian for H_{s2} can be approximately expressed as

$$\hat{H}_2 = \sum_m \left[t_{m,m+1} \left(c_m^\dagger c_{m+1} + \text{H.c.}\right) + \Delta_m c_m^\dagger c_m\right]. \tag{8}$$

As is shown, the introduction of the weak long lattice can modulate both the nearest-neighbor hoppings and on-site energies. Specifically, the modulation to the nearest-neighbor hopping rates is approximately given by

$$\begin{aligned} t_{m,m+1} &= \int dx W^*(x - x_m) H_{s2} W(x - x_{m+1}) \\ &= -\frac{V_2}{2} \int dx W^*(x - x_m) \cos(2k_2 x + \varphi) \\ &\quad \cdot W(x - x_{m+1}) \\ &= -t_1 \cos(2\pi\beta m + \varphi) + t_2 \sin(2\pi\beta m + \varphi), \end{aligned} \tag{9}$$

with $\beta = k_2/k_1$ being the commensurability parameter,

$$\begin{aligned} t_1 &= \frac{V_2}{2} \int dx W^*(x) \cos(2\beta k_1 x) W(x - 1), \\ t_2 &= \frac{V_2}{2} \int dx W^*(x) \sin(2\beta k_1 x) W(x - 1). \end{aligned} \tag{10}$$

The modulation to the on-site energies is approximately given by

$$\begin{aligned}\Delta_m =& \int dx W^*(x-x_m) H_{s2} W(x-x_m) \\ =& V_2 \int dx W^*(x-x_m) \frac{1-\cos(2k_2 x+\varphi)}{2} \\ & \cdot W(x-x_m) \\ =& \Delta \cos(2\pi\beta m+\varphi) + \text{c.e.}, \end{aligned} \tag{11}$$

with

$$\Delta = -\frac{V_2}{2} \int dx W^*(x) \cos(2\beta k_1 x) W(x), \tag{12}$$

where c.e. denotes a constant energy which can be safely neglected without affecting the main physics.

Combining Eqs. (5) and (8), we realize that the optical superlattice system in the tight-binding limit naturally implements the generalized AAH model,

$$\begin{aligned}\hat{H}_{\text{GAAH}} = \sum_m & \left[(t_0 + V_m^{\text{od}})\left(c_m^\dagger c_{m+1} + \text{H.c.}\right)\right. \\ & \left. + V_m^{\text{d}} c_m^\dagger c_m\right]. \end{aligned} \tag{13}$$

This contains the off-diagonal and diagonal modulations, i.e., $V_m^{\text{od}} = -t_1\cos(2\pi\beta m+\varphi)+t_2\sin(2\pi\beta m+\varphi)$ and $V_m^{\text{d}} = \Delta\cos(2\pi\beta m+\varphi)$. Note that the derivation of H_{GAAH} is based on the assumption $V_1 \gg V_2$ and using the approximated Wannier functions; hence, H_{GAAH} is not the exact Hamiltonian. However, it can be used to capture the main physical features.

Previous studies have focused on an extreme case which ignores the periodic modulations on the nearest-neighbor hoppings.[22,23,40] This leads to the standard AAH model Hamiltonian

$$\hat{H}_{\text{AAH}} = \sum_m \left[t_0\left(c_m^\dagger c_{m+1} + \text{H.c.}\right) + V_m^{\text{d}} c_m^\dagger c_m\right], \tag{14}$$

which contains only diagonal modulations. By associating the laser phase φ with the momentum k_y, the commensurability parameter β, and the magnetic flux, the standard AAH model can be precisely mapped to the two-dimensional lattice model describing the integer quantum Hall (IQH) effects, i.e.,

$$\begin{aligned}\hat{H}_{\text{IQH}} = \sum_{m,n} & [t_0 c_{m,n}^\dagger c_{m+1,n} + t_y e^{i2\pi\beta m} c_{m,n}^\dagger c_{m,n+1} \\ & + \text{H.c.}], \end{aligned} \tag{15}$$

where $t_y = \Delta/2$. Thus, the standard AAH model inherits the topological properties of the IQH states.

Topological Phase Diagrams and Edge States. Now, we show that the topological properties of the generalized AAH model are quite different from the standard AAH model. The topological origin of the one-dimensional generalized AAH model also comes from a two-dimensional system. We first study the topological properties of the energy bands in a synthetic two-dimensional momentum space. By applying a Fourier transform along the genuine lattice direction, the Hamiltonian for the generalized AAH model becomes $H_{\text{GAAH}}(k_x,\varphi)$. By scanning the relative laser phase φ from $-\pi$ to π and employing it as a synthetic dimension, a synthetic two-dimensional momentum space is built. Similar to the standard AAH model, for $\beta = 1/q$ ($q \in Z$), in the energy spectrum $E(k_x,\varphi)$ there are q energy bands. The topological property for the nth energy band is characterized using a synthetic Chern number, defined as

$$C_n = \frac{1}{2\pi}\int_{-\pi/q}^{\pi/q} dk_x \int_{-\pi}^{\pi} d\varphi F_n(k_x,\varphi), \tag{16}$$

where $F_n(k_x,\varphi)$ is the Berry curvature associated with the Bloch wave function $|\Psi_n(k_x,\varphi)\rangle$ corresponding to the nth energy band. Numerically calculating the Chern numbers allows us to obtain the full topological phase diagram of $H_{\text{GAAH}}(k_x,\phi)$.

Figure 2(a) presents the corresponding topological phase diagram for an odd q. We take $q = 3$ as an example. Each unit cell, in this case, has three sites. Thus, the system supports three energy bands. As is shown, compared to the standard AAH model having a single topological phase,[22,23] the generalized AAH model exhibits four different topological phases. According to the Chern numbers of the three energy bands (from the bottom to the top), the four topological phases are identified as ($C_1 = 1$, $C_2 = -2$, $C_3 = 1$) in phases I, ($C_1 = -2$, $C_2 = 1$, $C_3 = 1$) in phase II, ($C_1 = -2$, $C_2 = 4$, $C_3 = -2$) in phase III, and ($C_1 = 1$, $C_2 = 1$, $C_3 = -2$) in phase IV. In contrast, the standard AAH model ($t_1 = t_2 = 0$) possesses a single topological phase,[22,23] and the corresponding Chern numbers are ($C_1 = 1$, $C_2 = -2$, $C_3 = 1$), similar to phase I in the generalized AAH model.

Moreover, as illustrated in Fig. 2(a), the generalized AAH model features a variety of topological phase transitions. The transitions between different nontrivial topological phases, signified by the change of Chern numbers, are accompanied by different energy gap closings. For example, the transition between phases I and II is accompanied by the closure of the first energy gap (blue solid line), as shown by the change of the Chern numbers from ($C_1 = 1$, $C_2 = -2$) to ($C_1 = -2$, $C_2 = 1$) and the invariance of the Chern number C_3. Since the sum of the Chern numbers for all energy bands needs to be zero, the sum of C_1 and C_2 remains unchanged when crossing the topological phase transition. Similarly, the transition between phases II and III corresponds to the closure of the second energy gap (red dash-dotted line), as indicated by the change of the Chern numbers from ($C_2 = 1$, $C_3 = 1$) to ($C_2 = 4$, $C_3 = -2$) and the invariance of their sum. Although

the first and second energy gaps close for the transition between phases I (Ⅱ) and Ⅲ (Ⅳ), the specific changes for the three Chern numbers are determined by the zero-sum rule.

According to the bulk-edge correspondence, these nontrivial synthetic Chern numbers guarantee the appearance of topological edge states at the boundaries of the actual dimension. In Fig. 2(b), we numerically calculate the energy spectra of the one-dimensional generalized AAH model in phase I, under the open boundary condition, as a function of φ. As depicted in Figs. 2(c), the modes in the energy gaps are the left and right edge states, maximally localized at the left and right edges, respectively. It is a characteristic of the edge state that the gap's topology determines the energy gap. For example, for the nth energy gap, its topology is characterized by the topologically invariant $C_n^{\rm gap} = \sum_{i=1}^{n} C_i$, related to the topology of the energy bands below this gap. Consequently, the number and group velocity of the edge states in this energy gap is respectively determined by the amplitude and sign of $C_n^{\rm gap}$. Figure 2(b) illustrates that $C_1^{\rm gap} = 1$ for the first energy gap. Thus, there is one left and right edge state in this gap. However, for the second energy gap, $C_1^{\rm gap} = -1$, the number of the corresponding left and right edge states are the same but with opposite group velocities. This bulk-edge correspondence can also be observed in the energy spectra of the edge states for phases Ⅱ–Ⅳ, as shown in Figs. 2(d)–2(f), respectively.

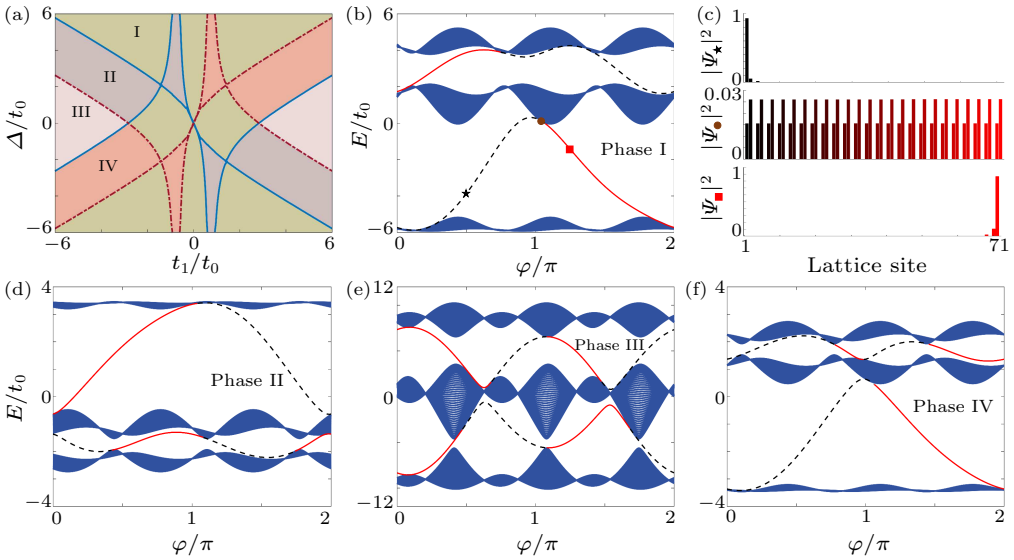

Fig. 2. (a) Topological phase diagram in the t_1 and Δ parameter spaces for $\beta = 1/3$. The topological phase transitions occur on closing the first (blue solid line) or second (red dash-dotted line) energy gaps. The energy spectra of the edge states for the generalized AAH model in phase I–Ⅳ are shown in (b) and (d)–(f). (c) The density distributions for the three modes marked in (b), showing that the black dashed and red solid lines in (b) and (d)–(f) correspond to the left and right states, respectively. The parameters used in the numerical calculations are (b) $t_1 = 2t_0$, $\Delta = 4t_0$, (d) $t_1 = -t_0$, $\Delta = 2t_0$, (e) $t_1 = 5t_0$, $\Delta = t_0$ and (f) $t_1 = t_0$, $\Delta = 2t_0$. The other parameter is $t_1 = t_2$, and t_0 is used as the energy unit.

Figure 3(a) further investigates the topological phase diagram for the generalized AAH model when q is even. As is displayed, the topological phases emerging and the topological phase transitions become much richer. More interestingly, we find a significant difference from the standard AAH model in this case. As presented before, the two middle energy bands in the standard AAH model for an even q are gapless;[22,23] whereas the corresponding two bands are gapped with nontrivial topology in the generalized AAH model. Specifically, for $q = 4$, there are six different gapped topological phases for the four energy bands, distinguished by the Chern numbers ($C_1 = 1$, $C_2 = 1$, $C_3 = -3$, $C_4 = 1$) in phase I, ($C_1 = -3$, $C_2 = 5$, $C_3 = -3$, $C_4 = 1$) in phase Ⅱ, ($C_1 = 1$, $C_2 = -3$, $C_3 = 1$, $C_4 = 1$) in phase Ⅲ, ($C_1 = -3$, $C_2 = 1$, $C_3 = 1$, $C_4 = 1$) in Ⅳ, ($C_1 = 1$, $C_2 = 1$, $C_3 = 1$, $C_4 = -3$) in phase V and ($C_1 = 1$, $C_2 = -3$, $C_3 = 5$, $C_4 = -3$) in phase Ⅵ. As shown by the closure of the three energy gaps in Fig. 3(a), this case generates more topological phase transitions. The bulk-edge correspondence is examined in Figs. 3(c)–3(h). As is indicated, these topological phases yield various forms of in-gap edge states. In contrast, the standard AAH model features a single topological phase,[22,23] where the two middle energy bands are gapless. The other two gapped energy bands are topologically nontrivial with $C_1 = 1$ and $C_4 = -1$, respectively, manifested in Fig. 3(b) by the touching central band and a pair of edge states in the bottom and top energy gaps.

The topological properties of the generalized AAH model can be understood by mapping it to the two-

dimensional lattice model,

$$\hat{H}_{\mathrm{GIQH}} = \sum_{m,n} \big[t_0 c^{\dagger}_{m,n} c_{m+1,n} + t_y e^{i2\pi\beta m} c^{\dagger}_{m,n} c_{m,n+1} - t'_y e^{i2\pi\beta m} \big(c^{\dagger}_{m,n} c_{m+1,n+1} + c^{\dagger}_{m,n} c_{m-1,n+1} \big) + \mathrm{H.c.} \big], \tag{17}$$

where $t'_y = (t_1 + it_2)/2$. In this mapping, we perform a Fourier transformation to the synthetic momentum φ and transfer $H_{\mathrm{GAAH}}(\varphi)$ into two-dimensional real spaces. Compared to the lattice model in Eq. (15) describing the standard IQH effect, the above lattice model supports next-nearest-neighbor hoppings in the presence of magnetic fields. Consequently, this model depicts a generalized IQH effect, and the corresponding topological phases in the generalized AAH model belong to the A class irrespective of any symmetry.

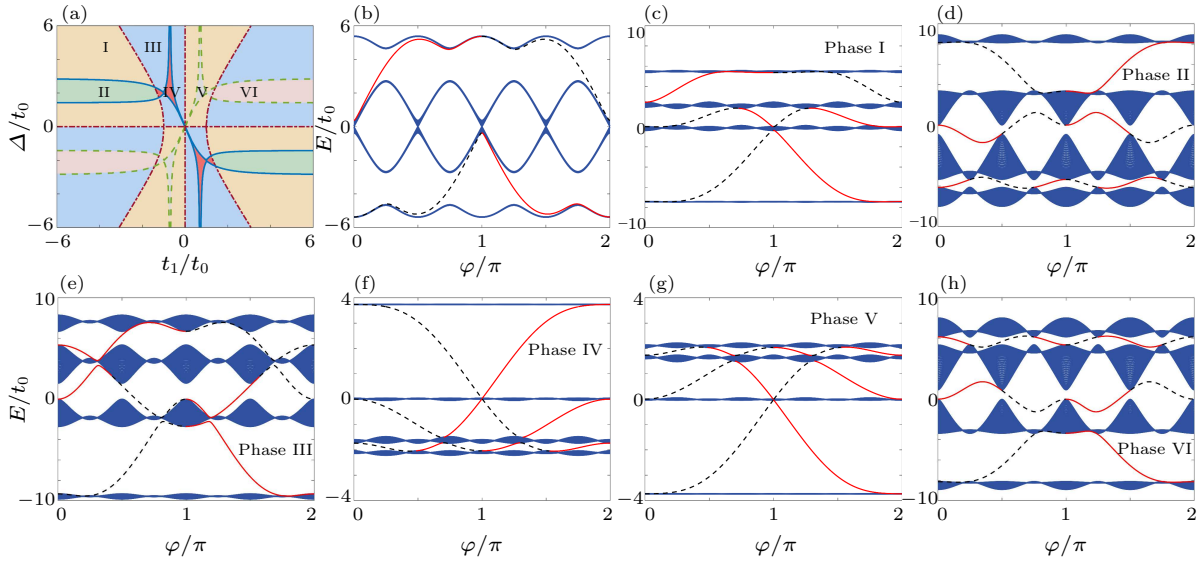

Fig. 3. (a) Topological phase diagram in the t_1 and Δ parameter spaces for $\beta = 1/4$. Different topological phases are separated by closing the first (blue solid line), second (red dash-dotted line) or third (green dashed line) energy gaps. The energy spectra of the edge states for the standard AAH model and the generalized AAH model in phases I–VI are shown in (b) and (c)–(h), respectively. The parameters are (b) $t_1 = 0$, $\Delta = 5t_0$, (c) $t_1 = 2t_0$, $\Delta = 5t_0$, (d) $t_1 = 4t_0$, $\Delta = -2t_0$, (e) $t_1 = 4t_0$, $\Delta = 4t_0$, (f) $t_1 = 0.8t_0$, $\Delta = -2t_0$, (g) $t_1 = 0.8t_0$, $\Delta = 2t_0$ and (h) $t_1 = 4t_0$, $\Delta = 2t_0$. The other parameter is $t_1 = t_2$.

Before the summary, we briefly discuss the detection of the topological phases in the generalized AAH model. As studied before, the optical superlattice system constitutes an ideal platform for implementing quantized topological pumping.[47–58] Suppose that our system is tuned into the regime where the ground band supports the topological phase with the Chern number C, via adiabatically scanning the relative laser phase φ over one period, one can implement a quantized topological pumping, where the atomic cloud's displacement is equal to C and detect the topological invariance. Another signature associated with topological phases is the appearance of an edge state at the systems' boundaries. By engineering a laser to create boundaries or interfaces in optical lattices and tuning the filling factor, the edge states in different energy gaps and their dynamics can be directly observed through time of flight[59,60] or Bragg spectroscopy technology.[61]

Summary and Outlook. We have shown that the optical superlattice system in the limiting case $V_1 \gg V_2$ implements the generalized AAH model, with periodic modulations on both the on-site energies and nearest-neighbor hoppings. We have demonstrated that this system supports much richer topological properties absent in the standard AAH model by calculating the topological invariants and edge states.

As is shown, the generalized AAH model provides opportunities to go beyond what is possible in the standard AAH model. For example, soon, it would be quite interesting to generalize our result to two dimensions for implementing a two-dimensional generalized AAH model. By introducing the relative laser phases in the two directions as two synthetic momentums, this model enables the implementation of four-dimensional topological phases,[62,63] and allows us to explore a variety of previously challenging four-dimensional topological phase transitions. Moreover, the generalized AAH model in the incommensurate case can also set a stage for controlling the Anderson localization.[25,64]

Acknowledgment. This work was supported by the National Key Research and Development Program of China (Grant No. 2017YFA0304203), the National Natural Science Foundation of China (Grant Nos. 12034012 and 12074234), the Changjiang Schol-

ars and Innovative Research Team in University of Ministry of Education of China (PCSIRT) (Grant No. IRT_17R70), the Fund for Shanxi 1331 Project Key Subjects Construction, and 111 Project (Grant No. D18001).

References

[1] Goldman N, Budich J C and Zoller P 2016 *Nat. Phys.* **12** 639
[2] Zhang D W, Zhu Y Q, Zhao Y X, Yan H and Zhu S L 2019 *Adv. Phys.* **67** 253
[3] Cooper N R, Dalibard J and Spielman I B 2019 *Rev. Mod. Phys.* **91** 015005
[4] Boada O, Celi A, Latorre J I and Lewenstein M 2012 *Phys. Rev. Lett.* **108** 133001
[5] Celi A, Massignan P, Ruseckas J, Goldman N, Spielman I B, Juzeliūnas G and Lewenstein M 2014 *Phys. Rev. Lett.* **112** 043001
[6] Mancini M, Pagano G, Cappellini G, Livi L, Rider M, Catani J, Sias C, Zoller P, Inguscio M, Dalmonte M and Fallani L 2015 *Science* **349** 1510
[7] Stuhl B K, Lu H I, Aycock L M, Genkina D and Spielman I B 2015 *Science* **349** 1514
[8] Chalopin T, Satoor T, Evrard A, Mahkalov V, Dalibard J, Lopes R and Nascimbene S 2020 *Nat. Phys.* **16** 1017
[9] Wall M L, Koller A P, Li S, Zhang X, Cooper N R, Ye J and Rey A M 2016 *Phys. Rev. Lett.* **116** 035301
[10] Livi L F, Cappellini G, Diem M, Franchi L, Clivati C, Frittelli M, Levi F, Calonico D, Catani J, Inguscio M and Fallani L 2016 *Phys. Rev. Lett.* **117** 220401
[11] Kolkowitz S, Bromley S, Bothwell T, Wall M L, Marti G E, Koller A P, Zhang X, Rey A M and Ye J 2017 *Nature* **542** 66
[12] Kanungo S K, Whalen J D, Lu Y, Yuan M, Dasgupta S, Dunning F B, Hazzard K R A and Killian T C 2022 *Nat. Commun.* **972**
[13] Meier E, An F and Gadway B 2016 *Nat. Commun.* **7** 13986
[14] Li Y, Zhang J, Wang Y, Du H, Wu J, Liu W, Mei F, Ma J, Xiao L and Jia S 2022 *Light Sci. Appl.* **11** 13
[15] Kang J H, Han J H and Shin Y 2020 *New J. Phys.* **22** 013023
[16] Wang D W, Liu R B, Zhu S Y and Scully M O 2015 *Phys. Rev. Lett.* **114** 043602
[17] Chen L, Wang P, Meng Z, Huang L, Cai H, Wang D W, Zhu S Y and Zhang J 2018 *Phys. Rev. Lett.* **120** 193601
[18] Cai H, Liu J, Wu J, He Y, Zhu S Y, Zhang J X and Wang D W 2019 *Phys. Rev. Lett.* **122** 023601
[19] He Y, Mao R, Cai H, Zhang J X, Li Y, Yuan L, Zhu S Y and Wang D W 2021 *Phys. Rev. Lett.* **126** 103601
[20] Mi C, Nawaz K S, Chen L, Wang P, Cai H, Wang D W, Zhu S Y and Zhang J 2021 *Phys. Rev. A* **104** 043326
[21] Fabre A, Bouhiron J B, Satoor T, Lopes R and Nascimbene S 2021 arXiv:2110.12971v1 [cond-mat.quant-gas]
[22] Lang L J, Cai X and Chen S 2012 *Phys. Rev. Lett.* **108** 220401
[23] Mei F, Zhu S L, Zhang Z M, Oh C H and Goldman N 2012 *Phys. Rev. A* **85** 013638
[24] Hofstadter D R 1976 *Phys. Rev. B* **14** 2239
[25] Aubry S and André G 1980 *Ann. Isr. Phys. Soc.* **3** 133
[26] Grempel D R, Fishman S and Prange R E 1982 *Phys. Rev. Lett.* **49** 833
[27] Modugno M 2009 *New J. Phys.* **11** 033023
[28] Biddle J, Wang B, Priour D J Jr and Sarma S D 2009 *Phys. Rev. A* **80** 021603(R)
[29] Biddle J, Priour D J Jr, Wang B and Sarma S D 2011 *Phys. Rev. B* **83** 075105
[30] Larcher M, Modugno M and Dalfovo F 2011 *Phys. Rev. A* **83** 013624
[31] Zhou L, Pu H and Zhang W 2013 *Phys. Rev. A* **87** 023625
[32] Qin P, Yin C and Chen S 2014 *Phys. Rev. B* **90** 054303
[33] Li X, Ganeshan S, Pixley J H and Sarma S D 2015 *Phys. Rev. Lett.* **115** 186601
[34] Li X, Pixley J H, Deng D L, Ganeshan S and Sarma S D 2016 *Phys. Rev. B* **93** 184204
[35] Cao Y, Xianlong G, Liu X J and Hu H 2016 *Phys. Rev. A* **93** 043621
[36] Yang C, Wang Y, Wang P, Gao X and Chen S 2017 *Phys. Rev. B* **95** 184201
[37] Li X, Li X and Sarma S D 2017 *Phys. Rev. B* **96** 085119
[38] Li X and Sarma S D 2020 *Phys. Rev. B* **101** 064203
[39] Yin H, Hu J, Ji A C, nas G J Liu X J and Sun Q 2020 *Phys. Rev. Lett.* **124** 113601
[40] Roati G, D'Errico C, Fallani L, Fattori M, Fort C, Zaccanti M, Modugno G, Modugno M and Inguscio M 2008 *Nature* **453** 895
[41] Kraus Y E, Lahini Y, Ringel Z, Verbin M and Zilberberg O 2012 *Phys. Rev. Lett.* **109** 106402
[42] Zeng Q B, Yang Y B and Xu Y 2020 *Phys. Rev. B* **101** 020201(R)
[43] Zeng Q B, Yang Y B and Xu Y 2020 *Phys. Rev. B* **101** 241104(R)
[44] Ganeshan S, Sun K and Sarma S D 2013 *Phys. Rev. Lett.* **110** 180403
[45] Cestari J C C, Foerster A and Gusmao M A 2016 *Phys. Rev. B* **93** 205441
[46] Liu T, Wang P and Gao X 2016 arXiv:1609.06939 [cond-mat.dis-nn]
[47] Lohse M, Schweizer C, Zilberberg O, Aidelsburger M and Bloch I 2016 *Nat. Phys.* **12** 350
[48] Nakajima S, Tomita T, Taie S, Ichinose T, Ozawa H, Wang L, Troyer M and Takahashi Y 2016 *Nat. Phys.* **12** 296
[49] Lu H I, Schemmer M, Aycock L M, Genkina D, Sugawa S and Spielman I B 2016 *Phys. Rev. Lett.* **116** 200402
[50] Lohse M, Schweizer C, Price H M, Zilberberg O and Bloch I 2018 *Nature* **553** 55
[51] Wang L, Troyer M and Dai X 2013 *Phys. Rev. Lett.* **111** 026802
[52] Mei F, You J B, Zhang D W, Yang X C, Fazio R, Zhu S L and Kwek L C 2014 *Phys. Rev. A* **90** 063638
[53] Wei R and Mueller E J 2015 *Phys. Rev. A* **92** 013609
[54] Ke Y, Qin X, Mei F, Zhong H, Kivshar Y S and Lee C 2016 *Laser Photon. Rev.* **10** 995
[55] Ke Y, Qin X, Kivshar Y S and Lee C 2017 *Phys. Rev. A* **95** 063630
[56] Hayward A, Schweizer C, Lohse M, Aidelsburger M and Meisner F H 2018 *Phys. Rev. B* **98** 245148
[57] Mei F, Chen G, Goldman N, Xiao L and Jia S 2019 *New J. Phys.* **21** 095002
[58] Chen Q, Cai J and Zhang S 2020 *Phys. Rev. A* **101** 043614
[59] Goldman N, Dalibard J, Dauphin A, Gerbier F, Lewenstein M, Zoller P and Spielman I B 2013 *Proc. Natl. Acad. Sci. USA* **110** 6736
[60] Leder M, Grossert C, Sitta L, Genske M, Rosch A and Weitz M 2016 *Nat. Commun.* **7** 13112
[61] Goldman N, Beugnon J and Gerbier F 2012 *Phys. Rev. Lett.* **108** 255303
[62] Kraus Y E, Ringel Z and Zilberberg O 2013 *Phys. Rev. Lett.* **111** 226401
[63] Price H M, Zilberberg O, Ozawa T, Carusotto I and Goldman N 2015 *Phys. Rev. Lett.* **115** 195303
[64] Ganeshan S, Pixley J H and Sarma S D 2015 *Phys. Rev. Lett.* **114** 146601